Chapter 5
Residual Stresses and Fatigue Life Enhancement of Cold Spray

H. Jahed and R. Ghelichi

5.1 Introduction

Residual stresses are referred to as stresses remaining in a structure in the absence of external mechanical or thermal loads. Trapped stresses such as stress in a preloaded bolt, which in most cases are due to elastic deformation (e.g., will be completely freed upon removal of preload), are also referred to as residual stresses. However, a more precise reference to residual stress is when elastic and plastic zones coexist within a structure free of external forces. Such stresses are induced where a stress gradient exists in a body and the stresses are larger than the elastic limit. Upon removal of external forces and to maintain the permanent deformation caused by the stress raiser, a self-balanced system of internal forces (residual stresses) remains in the structure. Therefore, residual stresses are usually local (next to the location of the stress concentration) and bounded by a large elastic region. Residual stresses are caused by most manufacturing processes such as welding, machining, and forming or are intentionally produced by processes like peening and autofrettage.

Tensile residual stresses are normally unwanted stresses that are induced because of manufacturing and/or joining processes, service overloads, and material defects. Tensile residual stress puts initial material flaws into an opening mode of fracture and hence promotes crack initiation and propagation, leading to a significant reduction in the life of the components. This type of residual stress is detrimental to the structure, and designers are normally trying to minimize or completely remove tensile residual stresses. Standard processes such as thermal stress relief are often used after manufacturing processes to remove unwanted residual stresses.

H. Jahed (✉)
Mechanical and Mechatronics Engineering Department, University of Waterloo, Waterloo, ON N2L 5H5, Canada
e-mail: hjahedmotlagh@uwaterloo.ca

R. Ghelichi
Department of Mechanical Engineering, Massachusetts Institute of Technology, Cambridge, MA 02139, USA

Compressive residual stresses, on the other hand, are beneficial. These types of stresses work against mode I crack initiation and delay formation and propagation of cracks. In most cases, the presence of the compressive residual stresses leads to the possibility of application of larger external loads and longer lives. Compressive residual stresses are normally intentionally made to enhance fatigue life. Established industrial processes like shot peening of aerospace and automotive parts, and autofrettage of pressure vessels are common examples of methods for creating beneficial compressive residual stresses.

Residual stresses can be produced by nearly every mechanical, chemical, and thermal process including coating technologies. Cold spray coating uses high particle velocity and impact energy to enable material coating on a substrate at a relatively low temperature. A by-product of cold spray coating is the formation of residual stress due to the peening effect of the particles' collision with the substrate. The high particle impact velocity causes high local stresses which lead to plastic deformation in the substrate in the proximity of the particle–substrate interface. Figure 5.1 depicts such plastic zone formation schematically. Due to the localized effect of the collision, the area that went under plastic deformation was surrounded by a large elastic domain resulting in the formation of local residual stresses. The dent resulting from the particle impact causes tension at the surface which upon unloading (adhesion of particle to surface) creates compressive residual stresses at and near the surface (Fig. 5.1). Such stresses are beneficial for fatigue life of the coated part. Due to the self-equilibrated nature of residual stress (i.e., zero net internal forces) associated with the compressive residual stress at and near the surface, there is tensile residual stress through the depth to balance off the residual force. A schematic pattern of the distribution of residual stress due to collision of a single particle with the substrate is shown in Fig. 5.1.
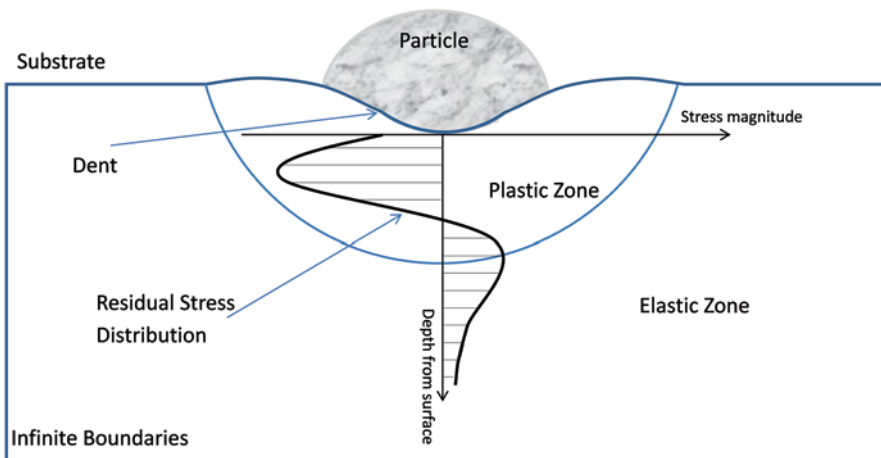

Fig. 5.1 Schematic of particle collision with the substrate in cold spray leading to formation of beneficial residual stress. Typical residual stress distribution at and near the surface is also shown. (Shayegan et al. 2014)

There have been a number of studies on the residual stress induced by cold spray coating. The recent literature is briefly reviewed here. McCune et al. (2000) have measured residual stresses for copper coatings, and Bagherifard et al. (2010a) performed X-ray diffraction (XRD) measurements on stresses induced in aluminum coatings. Ghelichi et al. (2012) measured the residual stress of different Al-alloy-coated samples and studied their effect on fatigue behavior. An interesting common observation in all studies is the relaxation of the compressive residual stresses at the interface of the coating and the substrate; conversely, the major difference is the reported stress in the substrate that is shown close to zero in McCune et al. (2000), whereas it is of a considerable amount, with respect to that of the deposited material, in other studies (Bagherifard et al. 2010a; Ghelichi et al. 2012). Price et al. (2006) studied the effect of the deposition of titanium on titanium. A Ti6Al4V alloy was coated with pure titanium by cold spray. Coatings were performed on as-received and grit-blasted (GB) samples. Fully reversed rotating bending fatigue of samples before and after coating revealed a 15 % reduction in fatigue endurance limit of the as-received samples, but no significant reduction was observed on the GB substrate. The reduction in fatigue endurance limit was attributed to the residual stress induced by the coating. However, in a study by Cizek et al. (2013), the cold spray of titanium on Ti6Al4V substrates was studied, and the average fatigue lives of cold-sprayed samples were reported to be shorter by 9 % when compared to the as-received uncoated specimens. Luzin et al. (2011) studied the residual stress in Cu- and Al-coated samples by neutron powder diffraction stress measurement. They used the Tsui and Clyne's progressive model (Tsui and Clyne 1997) that was originally developed to model the residual stress accumulation in thermal spray coatings to interpret their empirical results. Luzin et al. (2011) concluded that the residual stress is determined almost entirely by the plastic deformation process of the spray material due to the high-velocity impact of the particles and that the thermal effects do not play a notable role in changing the distribution of the induced stresses. Spencer et al. (2012) also followed the same approach using Tsui and Clyne's progressive model (Tsui and Clyne 1997) to understand the residual stress induced by cold-spraying Al and an Al alloy on Mg substrates. The residual stress distribution in their work was obtained by measurements using neutron diffraction with high spatial resolution. They concluded that the residual stress profile was more dependent on the alloy content, that is, intrinsic resistance to plastic deformation, than the spray-processing conditions. Sansoucy et al. (2007) studied the cold spray of Al–13Co–26Ce alloy particles on AA 2024-T3 substrate. They reported the fatigue and the bond strength of the Al–Co–Ce coatings. The results show that the Al–Co–Ce coatings improved the fatigue behavior of AA 2024-T3 specimens when compared to uncoated specimens. They attributed the increase in the fatigue properties to the residual compressive stresses induced in the coatings. Jeong and Ha (2008) investigated the effect of cold-spraying aluminum alloy A356 powder on the substrate made of the same material. They reported a significant 200 % improvement in the fatigue strength of the coated samples. The effect of cold spray coating on microstructure, residual stresses distribution, and fatigue life of Al5052 substrate coated with pure aluminum and Al7075 powders was studied by Ghelichi et al. (2012).

They reported a 30 % increase in the fatigue life of coated samples as compared to as-received samples when tested under a fully reversed cantilever-bending test. The increase in life was attributed to the presence of residual stress after the cold spray. The residual stress measurement in their work showed the peening effect of the coating on the substrate and verified the importance of the compressive residual stress on the fatigue life of the components. Moridi et al. (2014) studied the effect of cold spray of Al6082 by the same material on its fatigue life. They showed that the fatigue strength of coated samples was increased by 15 %. Ghelichi et al. (2014b) have studied, by experimental measurement and numerical simulation using the finite element method, the physical phenomenon of the residual stress inducement in the aluminum samples. They have shown that the process temperature has an annealing effect; that is, the gas temperature relieves the residual stress induced by particle impact. The numerical simulation by considering the annealing effect of the gas temperature matches with the experimental measurement. Shayegan et al. have studied the effect of aluminum powders on AZ31 by experiments and simulation. In the numerical simulation, both Ghelichi et al. (2014b) and Shayegan et al. (2014) have considered the randomness of the impacts. Shayegan et al. reported a 10 % increase in fatigue endurance and a maximum of 40 % life enhancement in the low-cycle fatigue of AZ31B extrusion when coated with AL1100.

A number of factors influence the residual stress level in cold spray coatings, including the impact velocity, particle size and hardness, particle temperature, quenching of the sprayed material due to high cooling rate, and thermal mismatch between the coating and the substrate. The recent studies on the residual stresses induced by cold spray coating can be categorized into: (1) experimental measurements of residual stress to quantify the level and deepness of these stresses; (2) numerical modeling of the impact and residual stresses; and (3) the influence of cold spray coating on the fatigue life. A brief review of approaches and details of the experimental measurement and numerical models of these three topics are provided in the following sections.

5.2   Experimental Measurement of Residual Stress in Cold Spray Coating

Constant bombardment of particles on the substrate and coating area is known as a major feature that results in increasing the residual stresses. The cold spray process is principally different from other types of thermal spray coating processes in terms of its lower process temperature and higher particle impact velocity, both of which directly affect the resulting residual stress distribution. The studies on quantifying residual stress in cold spray coating differ from one another because of either the method of measurements (layer removal, X-ray diffraction, or neutron diffraction) or the substrate/particle material (Al, Ti, Cu, or Mg).

McCune et al. (2000) have studied the residual stress of the cold spray coating of copper powders. The residual stress in the samples was measured using the layer

removal technique developed by Greving et al. (1994). The residual stress based on the depth from the outer surface was measured for different coated samples. To calculate the residual stresses from the released residual strain due to the removal of a layer, the modulus of elasticity of the material is needed. The measurement of Young's modulus was performed using the composite cantilever method of Rybicki et al. (1995). As expected, they found the residual stress to be compressive at and near the surface and tensile away from the surface. They have further noticed for the first time the effect of the temperature of the coating process as the annealing effect on the residual stress induced by the powders' impacts; that is, the residual stress has been reduced by increasing the coating temperature. Figure 5.2 shows the residual stress measurement of the coated samples presented by McCune.

Ghelichi et al. (2012, 2014a, b) have performed a series of studies on the coating residual stress measurement. To study the residual stress in-depth profile before and after the cold spray process, the XRD method was used. The analysis of the surface layer was performed using a diffractometer with radiation CrK_{α}, a circular irradiated area of 1 mm diameter, $Sin^2(\psi)$ method, and diffraction angle 2θ of 139° scanned between −45 and 45°. The effect of penetration depth of the radiation was approximately 5 μm. The in-depth measurements have been carried out step by step by removing a very thin layer of material (0.01/0.02 mm) using an electro-polishing device in order to obtain the in-depth profile of residual stresses. Different measurements have been performed in three rotation angles (0, 45, and 90°). They measured the residual stress induced by different aluminum particles on different aluminum alloy substrates. The coating samples included Al5052 substrate coated with Al7075 particles, and pure aluminum (size ranging from 10 to 40 μm). Figure 5.3 shows three different measurements of the coated samples for different aluminum alloy coating.

Ghelichi et al. (2014b) have performed a specific test to verify the annealing phenomenon in the coated samples. GB samples have gone under the coating process with the exact same temperature and pressure condition but with no powders. The coating temperature and time of the coating process for samples coated as with
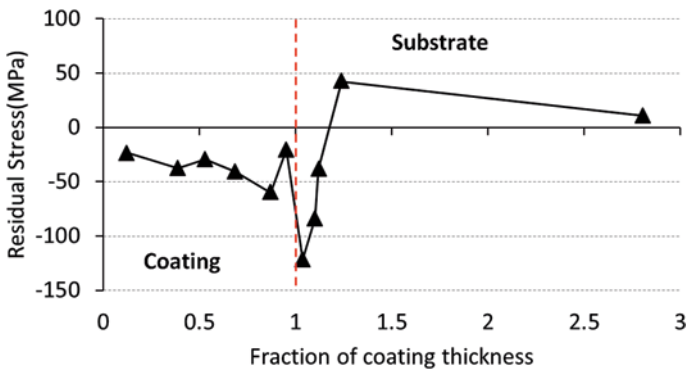

Fig. 5.2 Experimental measurement of the residual stress on copper-coated samples. (McCune et al. 2000; Ghelichi 2012)
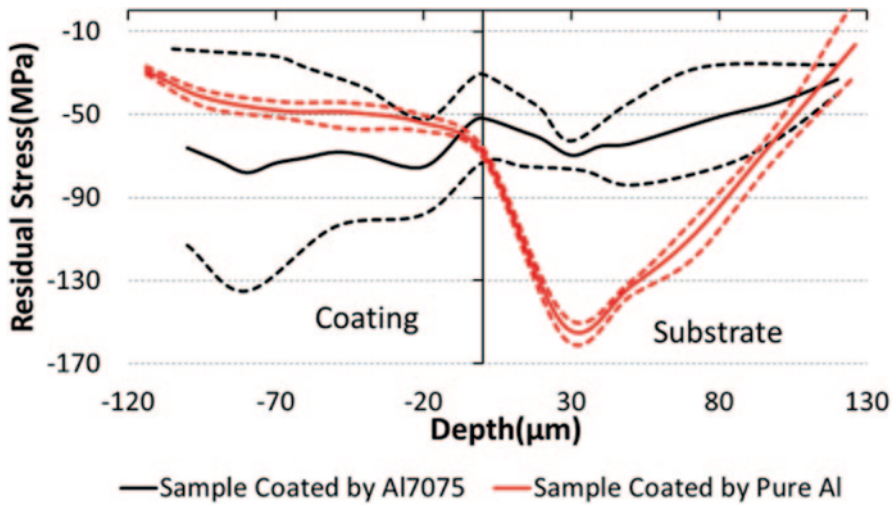
Fig. 5.3 Residual stress measurement for Al5052 samples coated with Al7075 and pure Al; *dashed lines* show the lower and upper bounds of measurements, and *solid lines* show an average value. (Ghelichi et al. 2014a)

Al7075 were 500 °C and 420 s, respectively, while for samples coated with pure Al were 350 °C and 90 s. Grit blasting will cause residual stress in the samples. The results show more time or temperature relieves more of the residual stress in the samples. The final results are shown in Fig. 5.4. By using this figure, Ghelichi et al. (2014a) estimated the annealing constants.

Shayegan et al. (2012), using the same XRD technique, have measured the residual stress for magnesium alloy substrate coated by aluminum powders. An air-quenched AZ31B extrusion piece was used as the substrate. The samples were first stress relieved using the American Society for Metals (ASM)-recommended method of thermal treatment of 260 °C for 15 min (1989) to remove residual stresses of the extrusion process. The substrate was then coated by commercially available
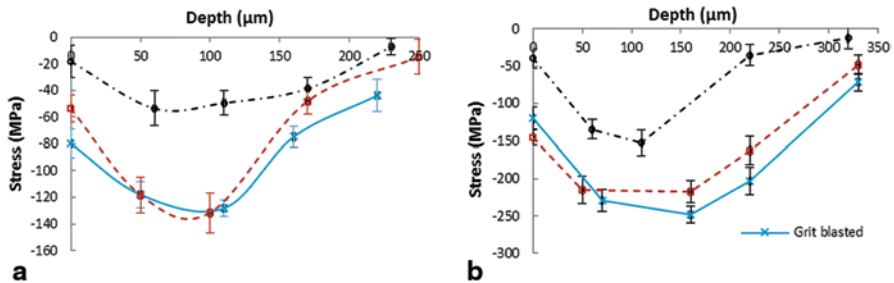

Fig. 5.4 The effect of coating temperature on relieving the residual stress in the samples: **a** Al5052, **b** Al6061. (Ghelichi et al. 2014b)
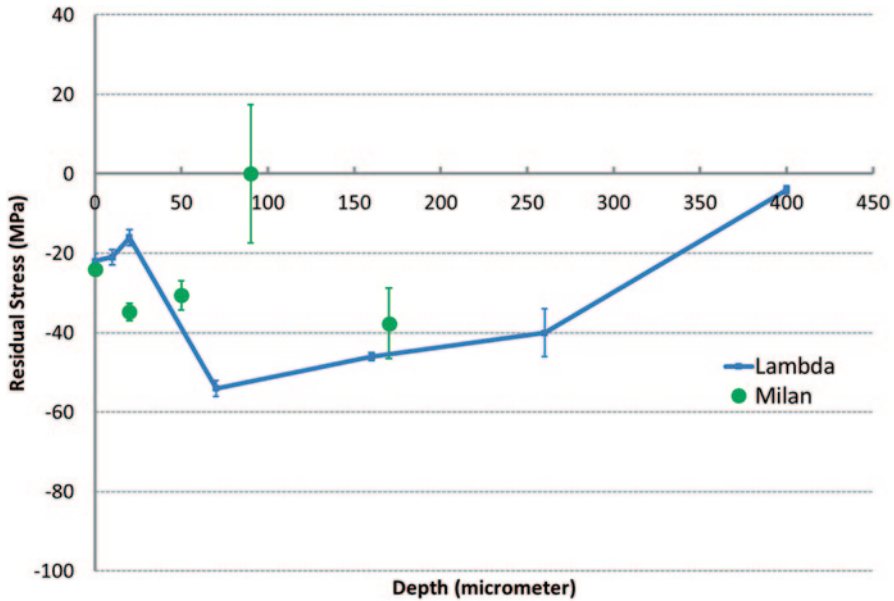
Fig. 5.5 Residual stress measurement for Al-coated AZ31 extrusion (Shayegan et al. 2014); the two sets of measurements were performed at Lambda Technologies and Polytechnic University of Milan

pure aluminum (Al>99.7%) powders with an average particle size of 25 µm. The sample surface was grit blasted before the cold spray with aluminum oxide. The following processing settings were used: temperature of 350 °C, pressure of 250 psi, and standoff distance of 12 mm. The coat displayed bond strength of 22 MPa, hardness of 34–37 HB, and density greater than 99.5%. XRD method was performed to measure the residual stresses at nominal depths of 10, 20, 70, 160, 260, and 400 µm in the extrusion direction. Figure 5.5 shows the experimental measurement of the residual stress.

The common aspects of all these measurements can be summarized in a few important facts. All different measurements show that compressive residual stresses are induced at the substrate surface. The level of this stress depends on material and coating parameters. The residual stress remains compressive beneath the surface and turns into tensile beyond that. The maximum compressive stress is the order of magnitude higher than the maximum in-depth tensile residual stress. The residual stress fades away beyond a few hundred microns of the substrate. The results also show that the residual stress will be relieved on the substrate; that is, the interface of the deposited materials and the substrate will experience less compressive residual stress as compared to both substrate and coating. This may be due to the high local plastic deformation and local grain size refinement of the interface (Ghelichi 2012). Finally, increasing the coating temperature will decrease the induced residual stress due to an annealing effect.

In this regard, the mathematical modeling using numerical simulation has been used in order to have a better perspective of this complex physical phenomenon. In the following section, two different models are reviewed in detail.

5.3 Numerical Modeling of a Cold Spray Process

Numeral simulations are used to provide a better understanding of different physical phenomena and to provide a tool for sensitivity and parameter analysis. They help qualitatively and, with an appropriate fitting, quantitatively to monitor different aspects of the process, especially when the size is small and deformation happens in a fraction of seconds where the experiment cannot capture every single detail. Simulation also helps in reducing the production cost by minimizing the number of experimental trials by providing some in-depth information on the effect of parameter changes on the final results.

In cold spray coating, the high-velocity impact of microparticles induces high local plastic deformation, which in turn induces compressive residual stress at and near the surface of the coated samples. Due to the high rate of impact velocity and flux of the particles on the substrate, the substrate experiences a very complex rate-dependent plastic deformation, which includes softening and localization in the material behavior (Champagne 2007).

There have been a number of efforts by researchers in simulating cold spray coating. Most of these researches are dedicated to the study of a single-particle impact in the coating process. These studies are focused on the effect of plastic behavior of the metallic substrate under a high-rate large local deformation due to the impact. Assadi et al. (2003) and Grujicic et al. (2014a), by choosing the Johnson–Cook plastic model, studied the single-particle impact. They have shown that the localization in stress–strain curvature can be the main reason for bonding the particles on the substrate. This theory has been backed up by experimental observation later on Ghelichi et al. (2011). Their study has been continued and modified by Kumar et al. (2009), Li et al. (2006), and Ghelichi et al. (2011). These studies were aimed at approximating the value of "critical velocity" which is the minimum velocity required to guarantee particle-to-surface bond. The latter references give a very good insight of the behavior of a particle in a single-particle impact shot. Few studies are focused on the response of the substrate due to multiple particle impacts. These studies have shown that the size and velocity of the particles are major factors altering the results in the process. In practice and in the real coating process, there is usually a broad distribution of the particle sizes with different velocities involved, which may be captured in simulation.

Here, in more detail, two studies are being reviewed. These two studies have considered the randomness of the particle size impact and different physical parameters that affect the plastic deformation and consequently the residual stress of the process. The studies by Ghelichi et al. (2014b) and Shayegan et al. (2014) are discussed here.

5.3.1 Residual Stress Due to Cold Spray of Aluminum Substrate

Ghelichi et al. (2014b) studied the residual stress of the two different aluminum alloys (Al5052 and Al6061) coated by Al7075. Due to the intrinsic similarity of the cold spray coating to shot peening, the model introduced by Bagherifard et al. (2010b) for shot peening simulation has been used.

One of the main constituents of cold spray simulation is the particle size distribution. To introduce the randomness of particle size, the Rosin–Rammler model (RosIn 1933; Ramakrishnan 2000; Eq. 5.1), which has been often used to estimate the particle distribution (Allen 2003; Li et al. 2006), was adopted. In Eq. 5.1, the cumulative density function (CDF), D_p is the particle diameter, and D_{rr} and Q are the Rosin–Rammler coefficients. The actual particle morphology of the powder used in the experiments was obtained through scanning electron microscope (SEM) images and then used to find the fitting parameters of the Rosin–Rammler model. Figure 5.6 shows a representative SEM image that was employed to obtain the particle histogram (Fig. 5.6b), which in turn yielded the Rosin–Rammler model parameters through fitting.

$$R(\text{CDF}) = \left\{ 1 - \exp\left[0\left(\frac{\ln(D_p)}{\ln(D_{rr})} \right)^Q \right] \right\} \times 100\%. \tag{5.1}$$

A uniform distribution was assumed for the position of the particles in the impact zone as shown by a red circle in Fig. 5.7. The number of particles has been calculated based on the thickness of the coated samples and average particle size.

Another major parameter in cold spray simulation is the particle velocity. In cold spray coating, which is a process with specified pressure and temperature, the particle velocity is a function of its diameter. To obtain an estimation of the impact velocity of particles with different sizes, based on the Dykuizen and Smith model (Grujicic et al. 2003), the relationship (Eq. 5.2) presented by Grujicic et al. (2004b) and Ghelichi et al. (2011) was adopted.
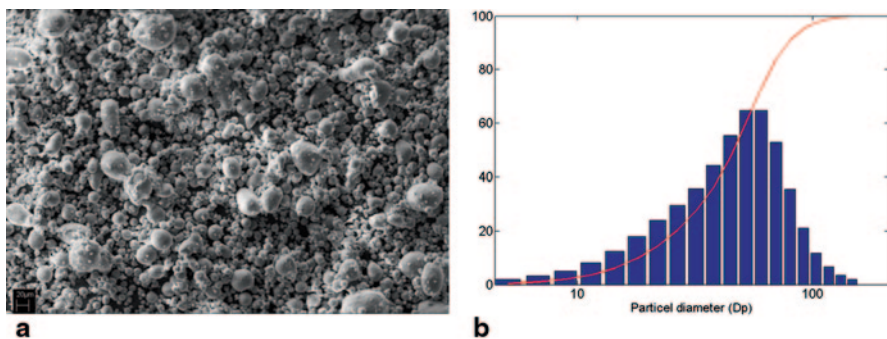

Fig. 5.6 a SEM image of Al7075 particle morphology and size distribution, **b** histogram and the CDF of the particle size distribution based on Rosin–Rammler (D_{rr}=45.95; Q=21.46). (Ghelichi et al. 2014b)
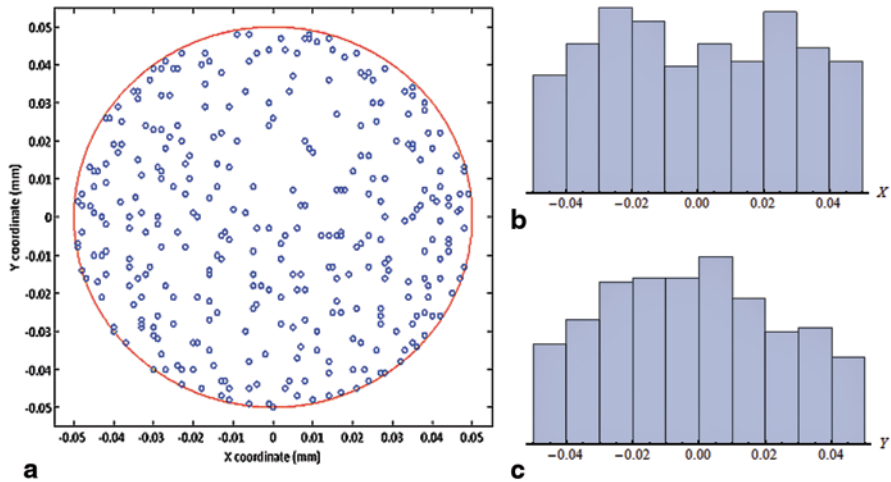
Fig. 5.7 a The center of the particles *(blue dots)* in one of the models with respect to the borders of the impact zone *(red circle)*; **b** and **c** show the histogram of distribution of the particles in x and y direction. (Ghelichi et al. 2014b)

$$V_{impact} = V_p e^{-\rho_{st}*L_{st}/4\rho_p D_p}$$

$$\rho_{st} = Re(-1.04 + 2.27M - 0.21M^2) \quad (5.2)$$

$$L_{st} = Re(0.97 - 0.02M)$$

In Eq. 5.2, V_{impact} is the velocity of the particles at the surface of the substrate at the time of impact and Re is the Reynolds number. The Mach number (M) and particle velocity (V_p) at the end of the cold spray nozzle can be calculated by Eqs. 5.3 and 5.4:

$$M = \left[\kappa_1 \frac{A}{A^*} + (1 - \kappa_1) \right]^{k_2}$$

$$\kappa_1 = 218.0629 - 243.5764\gamma + 71.7925\gamma^2 \quad (5.3)$$

$$\kappa_2 = -0.122450 + 0.28130\gamma$$

and

$$\frac{V_p}{V_e} = 0.5\left(\frac{V_p}{V_e}\right)_{18} + 0.5\left(\frac{V_p}{V_e}\right)_{20}$$

$$\left(\frac{V_p}{V_e}\right)_{20} = -e^{\frac{-9\mu x}{\rho_p D_p^2 V}} + 1$$

$$\left(\frac{V_p}{V_e}\right)_{18} = -e^{-\sqrt{\frac{3\rho_0 C_D x}{\rho_p D_p}}} + 1. \quad (5.4)$$

The gas velocity at the nozzle exit (V_e) and density of the gas (ρ_0) can be calculated by Eqs. 5.5 and 5.6. Gas viscosity (μ) may be evaluated using Sutherland's formula (Robert 1984; Dykhuizen and Smith 1998).

$$\rho_e = \frac{\rho_0}{(1+ \dfrac{\gamma- 1}{2} M^2)^{1/\gamma-1}}$$

$$V_e = M\sqrt{\gamma R T_e} \tag{5.5}$$

$$T_e = \frac{T_0}{1+ \dfrac{1- \gamma}{2} M^2}.$$

$$\rho_0 = \frac{P_0}{R T_0}$$

$$\mu= \mu_0\left(\frac{a}{b}\right)\left(\frac{T_e}{T_{S0}}\right)^{3/2} \tag{5.6}$$

$$a= 0.555T_0+ C; b= 0.555T+ C.$$

Another major constituent of cold spray particle impact simulation is the particle temperature. Papyrin et al. (2006) presented an analytical formulation for the particle temperature at the contact surface:

$$T_p = T_0+ C\exp\left(\frac{N_u \dfrac{6k}{d_p^2} x}{\rho_p \vartheta_p C_P}\right)\Big|_{x= \text{impact\ dist}}$$

$$N_u = 2a+ 0.459b Re^{0.55} Pr^{0.33} \tag{5.7}$$

$$a= \exp(-M)\left(1+ \frac{17M}{Re}\right)^{-1}, b= 0.666+ 0.333\exp\left(-\frac{17M}{Re}\right),$$

where k stands for thermal conductivity; Re is the Reynolds number for particles; C_p represents the heat capacity of the particles; $Pr= \dfrac{c_p \mu}{k}$ is the Prandtl number, where c_p is the specific heat, and μ is the dynamic viscosity obtained from Eq. 5.6.

Another significant constituent of the simulation is the material model for the substrate and particles. Considering that there is appreciable plasticity with high strain rate (impact) involved, proper plasticity models need to be adopted to mimic the characteristics of the deformation. In this study, a combined isotropic and kinematic hardening model (Lemaitre and Chaboche 1990) was chosen for the substrate and the Johnson–Cook model (Johnson and Cook 1983) presented in Eq. 5.8 was adopted for the powders. The material constants for the Al particles are presented in Table 5.1 (Brar et al. 2009).

Table 5.1 Mechanical properties of the material. (Johnson and Cook 1983)

Material	Hardness (Rock-well)	Density (kg/m³)	Specific heat (J/ kg °K)	Melting point (°K)	B_1 (MPa)	B_2 (MPa)	n	C	M
Al 7075-T6	87	2800	960	910	546	674	0.72	0.059	1.56

$$\sigma_{eq} = [B_1 + B_2 (\epsilon_p)^n][1 + Cln(\dot{\epsilon}_p / \dot{\epsilon}_{p0})] \times \left[1 - \left(\frac{T - T_{init}}{T_{melt} - T_{init}} \right)^m \right] \qquad (5.8)$$

Finally, a model for the annealing process of the particle and substrate after collision is required for the simulation. Due to the effect of the high temperature (close to annealing temperature) in the coating process, a phenomenon very similar to annealing may happen which releases the stress in the substrate (Totten 2002). The effect of time, as a main factor of annealing process, on residual stress relaxation can be modeled by adopting the Zener–Wert–Avrami function (Fine 1964):

$$\sigma^{rs} / \sigma_0^{rs} = \exp[-(St_a)^m] \qquad (5.9)$$

where m is a numerical parameter depending on the relaxation mechanism. Based on Eq. 5.9, in samples with the same geometry, volume, and material, when annealing parameters including time and temperature are the same, the fraction of $\sigma_0^{rs} / \sigma^{rs}$ remains constant. This constant has been applied as the annealing effect on numerical simulations' results to evaluate the final distribution of residual stresses.

5.3.1.1 Numerical Model Description

The commercial finite element software Abaqus/Explicit 6.12–1 Abaqus 6.12-1 (2012) was utilized to investigate multiple particle impact effects. A finite element (FE) model of the substrate and particles was created. Target mesh was set up by C3D8R 8-node linear brick elements with reduced integration and hourglass control. Due to the incompatibility of the very small size of the particles and large size/ volume of the substrate, and the localized effect of the impact, the bottom-side face of the substrate (target) was meshed by the half-infinite elements that provide quiet boundaries by minimizing the reflection of dilatational and stress waves back into the region of interest.

Figure 5.8a, b shows different views of the FE model. In this figure, the arrangement and the particle size distribution have been presented with respect to the red circle that represents the impact zone. The experimentally measured in-depth residual stress on the GB samples before the coating process has been considered as predefined stress field in the FE model before the particles impact. The numerical model was tuned for Al7075 powders and both Al5052 and Al6061 as the substrates.
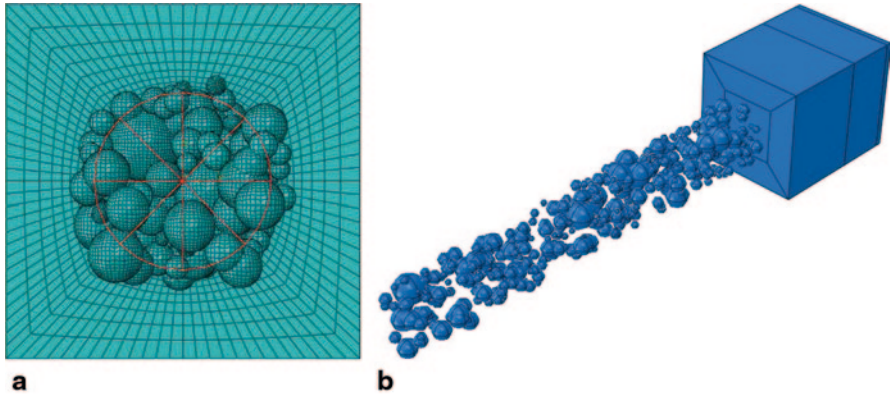
Fig. 5.8 a Top and **b** isometric view of the model developed for residual stress calculations (the *red* area represents the "impact-zone"). (Ghelichi et al. 2014b)

The results of the numerical simulation before and after considering the annealing effect of the temperature are presented in Fig. 5.9. It is clearly shown that results are improved when the effect of the process temperature on relieving the stress is considered. The numerical simulation and the experimental measurements confirm that in the cold spray coating process constant bombarding of particles induces residual stresses in the substrate. Although the process gas temperature is less than the melting point of the materials involved, it was shown to have a negative annealing effect on the favorable compressive residual stress induced by previous grit blasting and the particles' impact. This effect was clearly noted by means of experiments on samples formerly grit blasted and then submitted to the cold spray process without using powders. The results of the experimental measurements show the considerable effect of the process temperature on promoting residual stress relaxation.

A two-step approach aimed at realistically simulating the cold spray process was developed to obtain the final residual stress state in the substrate. It considers the residual stresses induced by grit blasting, particle size distribution, random impact position, and the corresponding velocity and temperature for the particles as a function of their size. The first step is based on an FE/explicit simulation and considers different material models compatible with the phenomenon. Even if some approximation is considered with respect to the real process (e.g., the bonding of the particles on the substrate is not considered in the modeling), the numerical model allows for studying the peening effect of the particles. The results obtained from the FE simulation do not consider the effect of the annealing. In this regard, in the second analytical step, the Zener–Wert–Avrami method (Fine 1964) was utilized to introduce the annealing effect on the numerical results using the experimental measurements performed on uncoated samples.
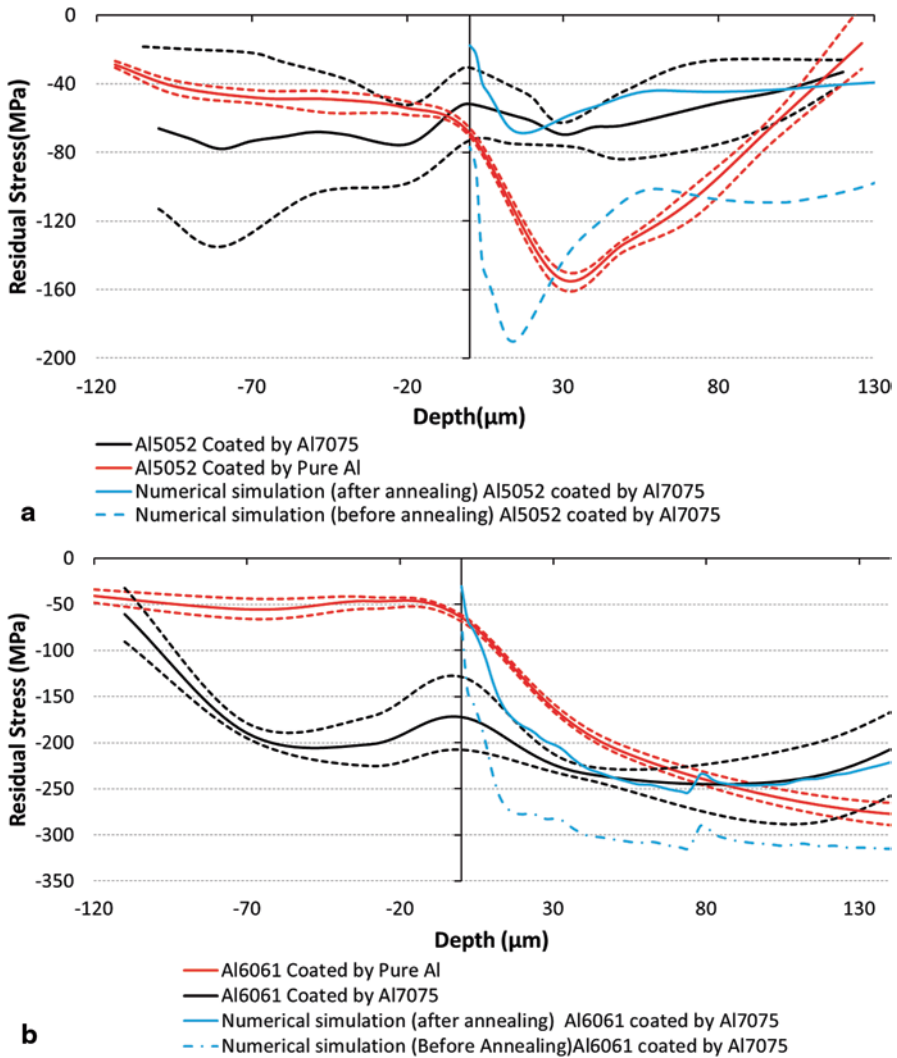
Fig. 5.9 Residual stress measurement for the coated samples with Al7075 and pure Al compared to the numerical simulation. **a** Al5052, **b** Al6061. (Ghelichi et al. 2014b)

5.3.2   Residual Stress Due to Cold Spray of Magnesium Substrate

Shayegan et al. (2014) presented the most recent numerical model. They simulated the coating of aluminum particles on magnesium (AZ31) extrusion substrate using LS-DYNA (LS-DYNA3D 1999) software. The focus of their study was the peening effect of the spraying and the resulting residual stress.

Magnesium extrusion has two main mechanical characteristics: (1) yield asymmetry and (2) directional anisotropy. Because of limited slip system in hexagonal close-packed (HCP) magnesium, deformation twinning is a major deformation mechanism when extension along the *c*-axis (basal axis) is induced. This results in a different deformation mechanism in tension and compression known as yield asymmetry. LS-DYNA (LS-DYNA3D 1999) material library provides MAT-124 that captures yield asymmetry by accepting two independent tensile and compressive stress–strain curves. Noting that yield asymmetry is the dominant deformation factor, and by ignoring the directional anisotropy of substrate, Shayegan et al. (2014) adopted MAT-124 in conjunction with the Cowper–Symonds (Eq. 5.11) strain rate model.

$$\frac{\sigma}{\sigma_0} = 1 + \left(\frac{\dot{\varepsilon}}{D}\right)^{\frac{1}{p}}, \tag{5.10}$$

where $\dot{\varepsilon} = \sqrt{\dot{\varepsilon}_{ij}\dot{\varepsilon}_{ij}}$ is the strain rate, σ is the von Mises stress, σ_0 is the semi-static yield stress and $D = 24,124$ and $p = 3.09$ (Najafi and Rais-Rohani 2011) are the strain rate parameters.

The tension and compression curves of AZ31B shown in Fig. 5.10 and other alloy parameters including density $(1770\,kg/m^3)$, Young's modulus (45 GPa), and Poisson's ratio (0.35) are used in the simulation.
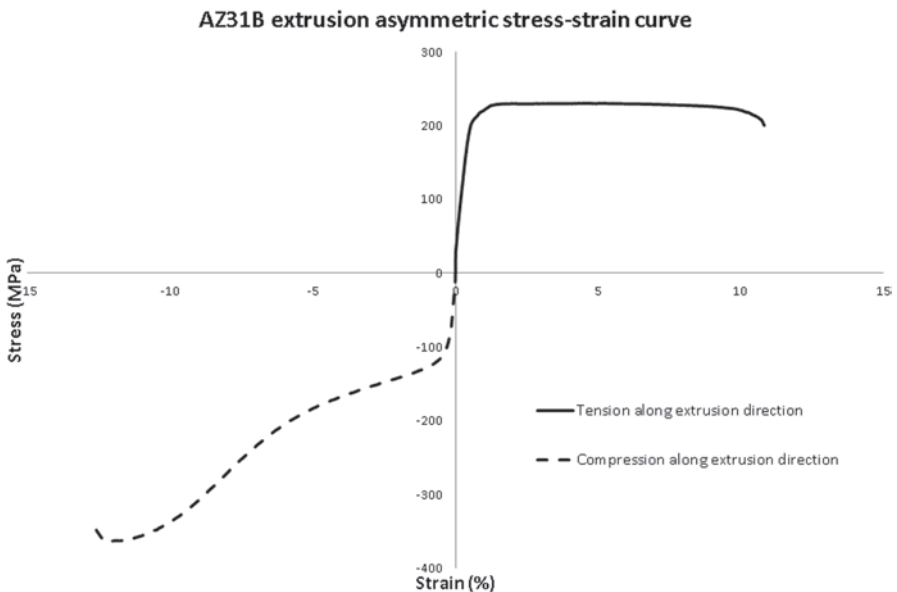

Fig. 5.10 Tension–compression curve of AZ31B. (Albinmousa et al. 2011)

Table 5.2 Johnson–Cook parameters for AL 1100-O. (Benck 1976; Pierazzo et al. 2008)

Value	Parameter
49	A (MPa)
157	B (MPa)
0.167	n
0.016	C
1.7	m
293	$T_{\text{room}}(K)$
933	$T_{\text{melt}}(K)$

The same Johnson–Cook material model (LS-DYNA MAT-15) as in Ghelichi et al. (2011) was used for aluminum particles which is suitable for problems with a high rate of strain with proper material softening due to adiabatic temperature increase (Table 5.2).

For the dissemination of stress waves due to high-velocity collision of particles to the work piece, the following Gruneisen (Albinmousa et al. 2011) equation is used:

$$p = \frac{\rho_0 C_0^2 \mu \left[1 + \left(1 - \frac{\gamma_0}{2} \right) \mu - \frac{a}{2} \mu^2 \right]}{\left[1 - (S_1 - 1)\mu - S_2 \frac{\mu^2}{\mu + 1} - S_3 \frac{\mu^3}{(\mu + 1)^2} \right]^2} + (\gamma_0 + d\mu) E; \ \mu = \frac{\rho}{\rho_0} - 1, \quad (5.11)$$

where C_0 is the bulk speed of sound, ρ_0 is the initial density, ρ is the current density, S_1, S_2, and S_3 are the coefficients of the slope of the $U_s - U_p$ curve, U_s is the shock wave velocity, U_p is the particle velocity, γ_0 is Gruneisen's gamma at the reference state, d is the first-order correction coefficient per volume for γ_0, and E is the internal energy per unit reference volume. Proper parameters of Gruneisen equation for Al 1100-O have been published by Group GMX-6, Los Alamos (1969; Table 5.3).

Other material constants of AL 1100-O particles that are used are density ($2710\ \text{kg/m}^3$), Young's modulus (70 GPa), Poisson's ratio (0.33), shear modulus (26 GPa), and specific heat capacity (890 J/kg K) (Fig. 5.11).

In this study, the randomness in the size and the shape of the particles have been considered. A distribution has been chosen based on the average size of the particles obtained from the powder morphology in the coating process and different shapes are given to the particles. The final results of the numerical model showing the distribution of residual stress at and near the surface of the substrate is presented in Fig. 5.12. Also shown in the same figure are the results of residual stress measurements of two sets of coated samples using XRD. Given the variability in the measurements, the simulation results are comparable to the measurements, especially at the surface of the substrate.

Table 5.3 Gruneisen equation of state parameters for AL 1100-O (1969)

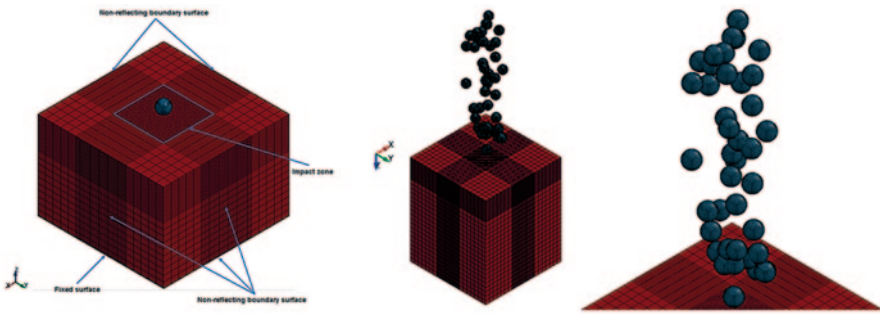| Value	Parameter
5328	C (m/s)
1.338	S_1
0	S_2
0	S_3
2	γ_0
0	A

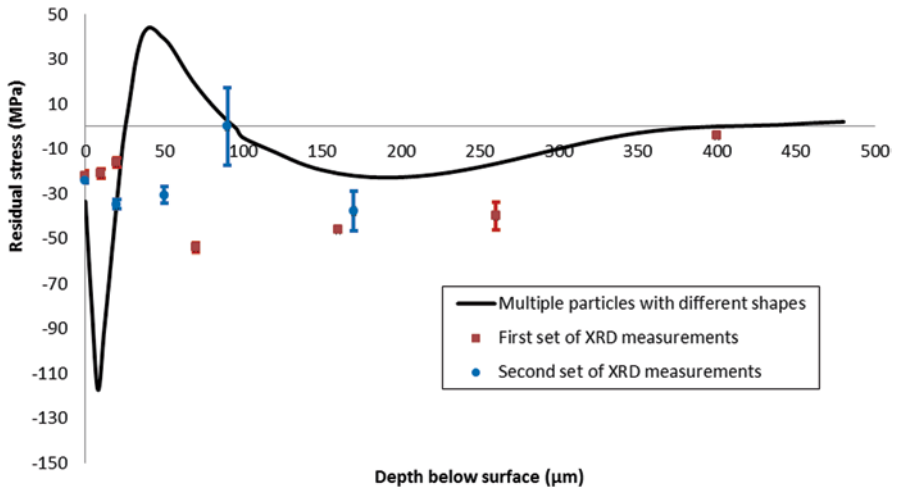**Fig. 5.11** Mesh configuration and developed finite element model. (Shayegan et al. 2014)

Fig. 5.12 Numerical results with Shayegan et al. (2014) model compared to experiments. *XRD* X-ray diffraction

5.4 Life Enhancement Resulting from Cold Spray Coating

The compressive residual stress on the surface will delay crack initiation and propagation and increase the fatigue endurance of the metallic components. Due to the presence of initial compressive stress, under service cyclic load, the maximum tensile stress stays at a very low value, and in some cases even at zero. Therefore, initial surface cracks are not subjected to the opening mode of crack propagation. Hence, the presence of the beneficial compressive residual stress prolongs the life or can allow for higher external loads to be applied. The formation of compressive residual stresses due to the peening effect of cold spray was discussed in details in the previous sections; we now focus on the life enhancement resulting from cold spray coating.

Ghelichi et al. (2012) studied the effect of cold spray coating on Al alloys using different powders and treatments. The specimen suggested by ASTM-B93 (2009) has been used for performing fatigue tests on samples shown in Fig. 5.13. The load control pure bending fatigue tests were performed using the specimen suggested by ASTM B-593 (2009). This standard suggests a fixed-cantilever, constant-deflection-type machine. The specimens are designed for the bending test based on the approach suggested by standard as presented in Fig. 5.13a along with a picture of the prepared specimen (Fig. 5.13b). The specimens were tested using a load control pure bending fatigue machine. Bending fatigue tests (stress ratio $R=-1$) have been carried out at room temperature at a nominal frequency of 90 Hz on as-received, GB, and other coated series of specimens. The specimens that passed ten million cycles were considered as run-out. The brief staircase method presented by Dixon and Massey (1969) has been used for performing the tests with a stress step of 10 MPa, and the Hodge–Rosenblatt (Dixon and Massey 1969) approach has been considered for calculating the fatigue endurance corresponding to 10 MPa. The fatigue test data have been elaborated based on ASTM standard E739–91 (2010) to obtain the S–N diagram for the different applied treatments.
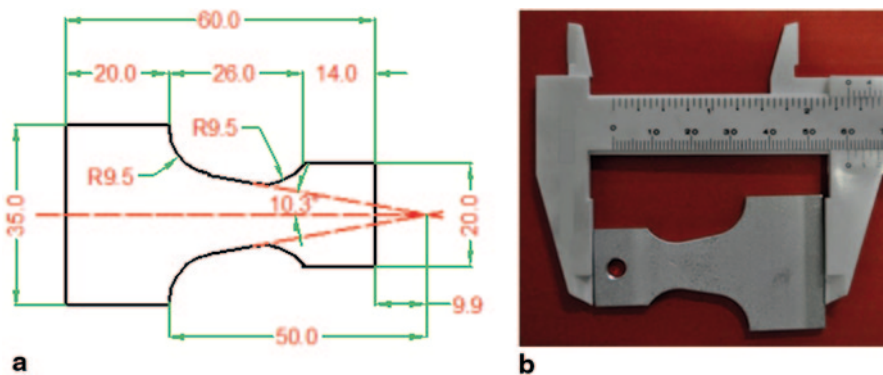

Fig. 5.13 Test specimen suggested by ASTM Standard B593-96 (2009), which has a uniform stress distribution under bending. **a** Detailed design of the specimen (all units in millimeter). **b** A view of a prepared specimen. (Ghelichi et al. 2012)
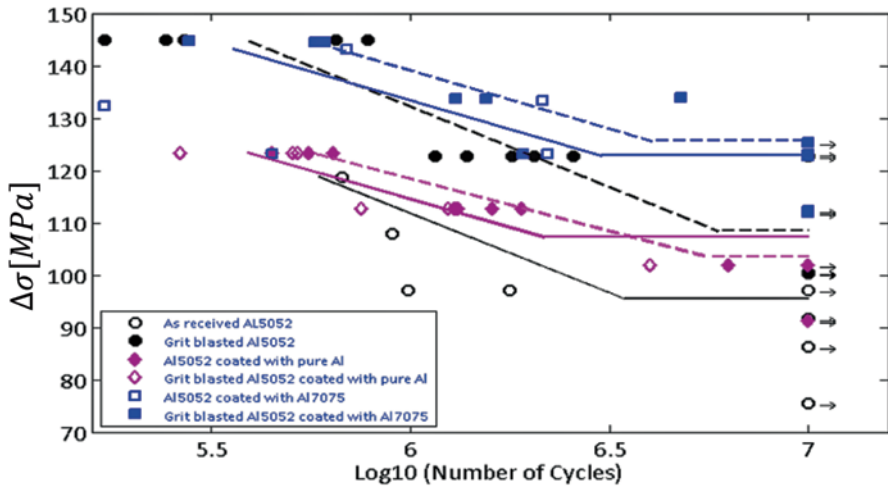
Fig. 5.14 The S–N diagram obtained from fatigue tests of coated and uncoated samples. (Ghelichi et al. 2012)

Two different types of aluminum powders have been coated by low-pressure cold spray coating (Cadney et al. 2008; Maev and Leshchynsky 2008) on both GB and as-received Al5052 in order to study the effect of the treatments on the fatigue endurance of the substrate. The specimens have been tested through a pure bending fatigue test. Residual stress measurement by XRD, microhardness tests, and SEM observations of fracture surfaces has been performed on the specimens. The results, presented in Fig. 5.14, show that the improvement in the fatigue life depends on the powders. The results prove that the residual stress due to grit blasting improves the fatigue endurance regardless of the powder and substrate, and an extra advantage can be obtained by choosing the appropriate powders.

Two main reasons have been mentioned for the life improvement, hardness of the particles, and the bonding of the deposited materials on the substrate. The microhardness test shows a great improvement in the hardness of the Al7075 with respect to the substrate. Incidentally, the grit blasting of the sample helped to increase the fatigue life; this improvement is mainly due to inducing extra residual stress in the substrate. SEM images (Fig. 5.15) show that the samples with higher fatigue endurance have a stronger bonding between the substrate and deposited materials.

Mahmoudi et al. (2012) and Kalatehmollaei et al. (2014) worked on fatigue improvement achieved by cold spray coating of magnesium substrate with aluminum alloys. For this purpose, cylindrical hourglass specimens of AZ31B extrusion have been used. Three groups of specimens including: as-received, stress-relieved, and stress-relieved/coated specimens have been tested by a rotating bending machine (RBM) to prepare S–N curves for each group. Comparing S–N curves provides an
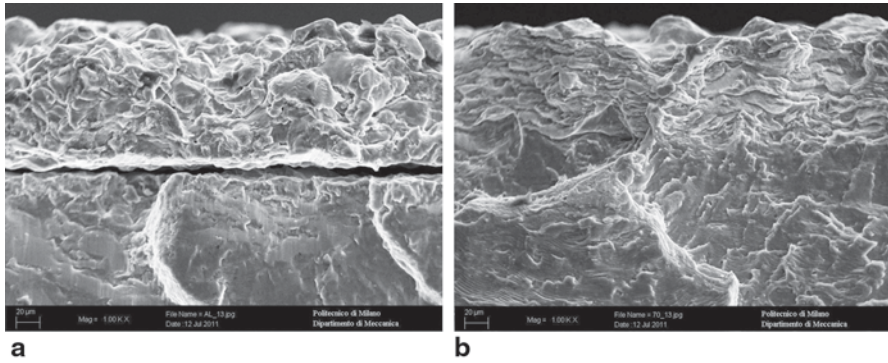
Fig. 5.15 SEM observation of the interface of the deposited material and the substrate in broken samples. **a** Sample coated by pure Al. **b** Sample coated by Al7075. (Ghelichi et al. 2012)

estimation of the effect of cold spray coating on the fatigue strength of AZ31B. All tests were performed at standard laboratory conditions. Tests were performed at frequencies between 50 Hz for low-cycle to 100 Hz for high-cycle tests. Specimens used for the test are shown in Fig. 5.16. The overall length of the specimens is 70 mm, and the diameter of the neck is 7 mm.

There was an initial compressive residual stress in as-received specimens due to the extrusion process of AZ31B. Using XRD measurement on a cylindrical specimen in the hourglass zone shows the amount of this compressive stress to be 43 MPa. As-received specimens have been used for fatigue tests to correlate the initial residual stress to fatigue life and to be able to compare results with other groups. A stress relief process was applied on the second group of AZ31B specimens. The ASM-recommended stress relief process, 500 °F (260 °C) for 15 min, was used for these specimens. The purpose is to evaluate the fatigue strength in absence of any residual stress. XRD measurement on stress-relieved cylindrical specimens on an hourglass area showed that the surface stress was removed. The purpose of selecting this group for fatigue tests is to evaluate the residual stress that is induced due to cold spray coating and its effect on the fatigue life of AZ31B. Stress-relieved
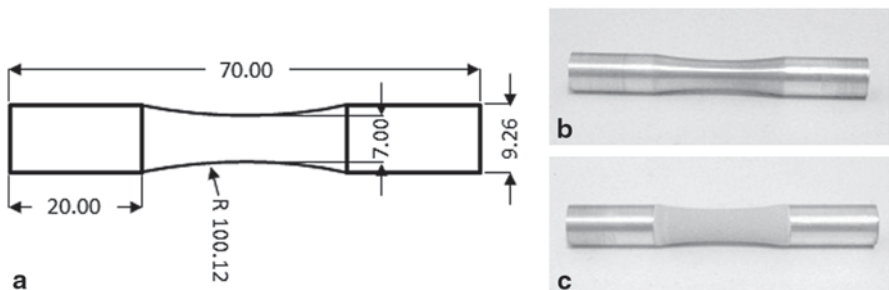

Fig. 5.16 Round specimens used for extracting S–N curve of AZ31B; **a** drawing, **b** uncoated, and **c** coated samples. (Kalatehmollaei et al. 2014)
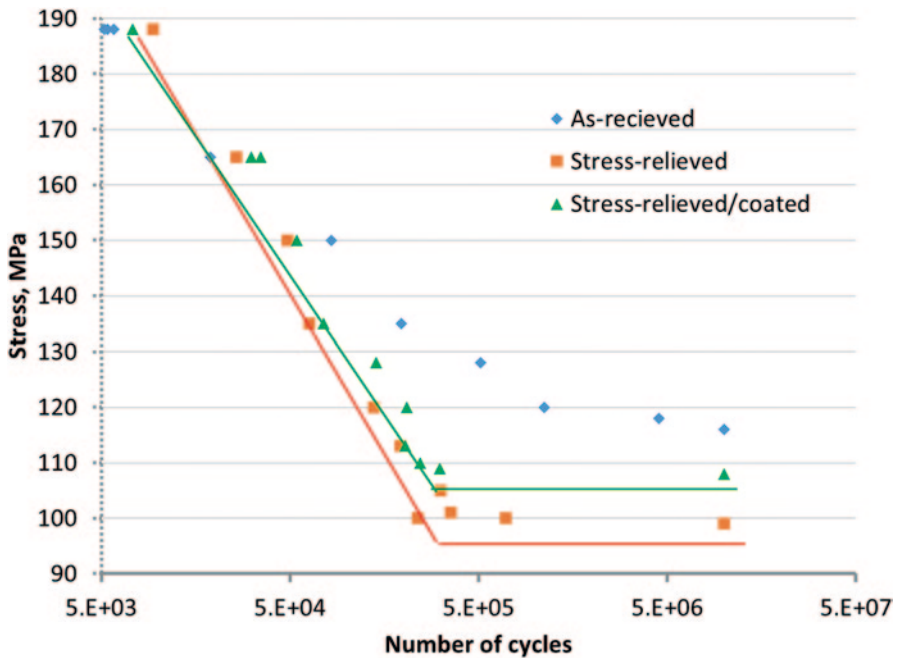
Fig. 5.17 S–N curves of as-received, stress-relieved, and stress-relieved/coated specimens of AZ31B. (Kalatehmollaei et al. 2014)

specimens have been coated with the following specifications and parameters: particle velocity =400 m/s, particle average diameter =40 μm, particle material of aluminum alloy, series 1100, grit blasting before cold spray coating, and coating layer thickness =0.1 mm. The coating has been applied on the hourglass area only. Figure 5.17 shows the S–N curve for three groups of specimens.

Figure 5.18 shows the fracture surface of a stress-relieved/coated specimen that has been tested under nominal stress of 188 MPa. As Fig. 5.18a presents, the crack initiation region is extended from the middle right to middle bottom of the image. Except for the crack initiation point (shown in the center of Fig. 5.18a), no coating layer delamination is observed around the fracture surface of the specimen; this observation proves strong bonding between coating particles and the specimen surface. Figure 5.18c shows the coating layer and the fracture surface.

As expected, there is a correlation between surface residual stress and fatigue strengths. Table 5.4 shows the values of surface residual stress, measured by XRD, and endurance limit for the three groups of specimens.

In low-cycle fatigue, there is a considerable drop in the fatigue life after stress relief. This is due to the considerable loss of compressive residual stress. Cold spray coating process improves the fatigue strength slightly. This means that the residual stress induced by cold spray coating is much lower than the residual stress induced by the initial extrusion process forming of the as-received specimens. The as-received specimens show better fatigue strength among the three groups. The S–N
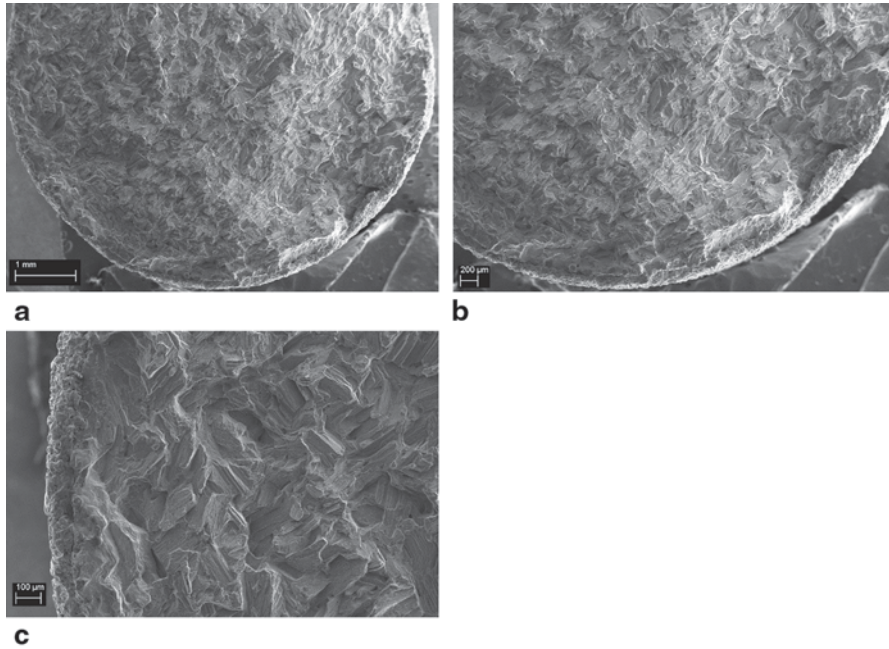
Fig. 5.18 Fracture surface of stress-relieved/coated specimen with the nominal stress of 188 MPa; **a** and **b** crack initiation region, **c** coating layer. (Mahmoudi 2012)

Table 5.4 XRD results on cylindrical specimens. (Cadney et al. 2008)

Group	Residual stress on surface (MPa)	Endurance limit (MPa)	Remarks
As-received	−43	116	Measured on hourglass area
Stress relieved	~0	99	Measured on hourglass area
Stress relieved/coated	−22	108	Measured on coated flat sample

curve for this group has a smooth transition to the endurance limit while the S–N curves of the stress-relieved and stress-relieved/coated specimens have sharp transitions to the endurance limit. The stress relief process lowers the endurance limit of the as-received specimens from 116 to 99 MPa, equal to 14.6%. The coating process improves the fatigue strength of stress-relieved specimens and increases their endurance limit from 99 to 108 MPa, equal to 9%.

In a different study, Cizek et al. (2013) performed fatigue tests for four different sets of samples. The same conclusion has been drawn regarding the grit blasting which can improve the fatigue limit of the samples. The 4-mm-thick Ti6Al4V sheets were cut into the shape shown in Fig. 5.19. Chemical degreasing was carried out in order to remove any oil or contaminant from the substrate surfaces. The samples have been grit blasted with SiC and Al_2O_3 particle.
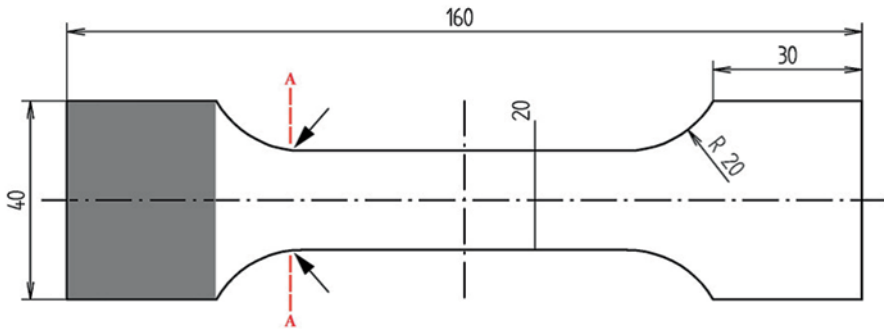
Fig. 5.19 Ti6Al4V samples used for cold spray coating. (Cizek et al. 2013)

Using the measured resonance frequencies from the fatigue experiments, the coating elastic moduli were obtained by a method described in Kovářík et al. (2008). Figure 5.20 shows the morphology of the surface of the different sets of the samples. The grit-blasting procedure produced a roughened surface (Ra~3 µm as compared to Ra = 0.82 µm of the as-received samples) and introduced abrasive angular Al_2O_3 and SiC particles into the Ti6Al4V material.

The final results show that cold spray deposition of Ti layers reduces fatigue life and causes the lowest values among the tested sets (91 % of the as-received set); it
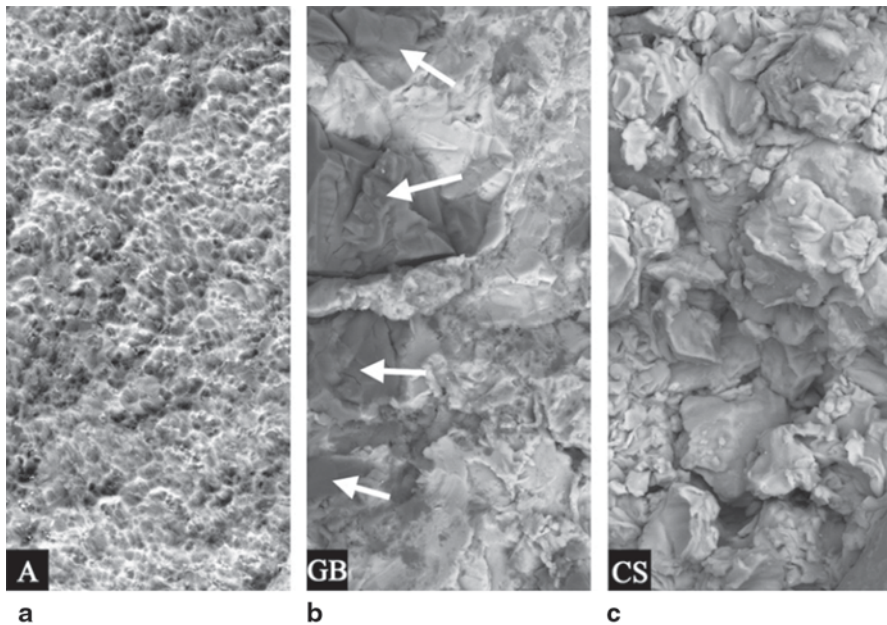

Fig. 5.20 Surface morphology of the **a** as-received *(A),* **b** grit-blasted *(GB),* and **c** cold-sprayed *(CS)* samples. (Cizek et al. 2013)
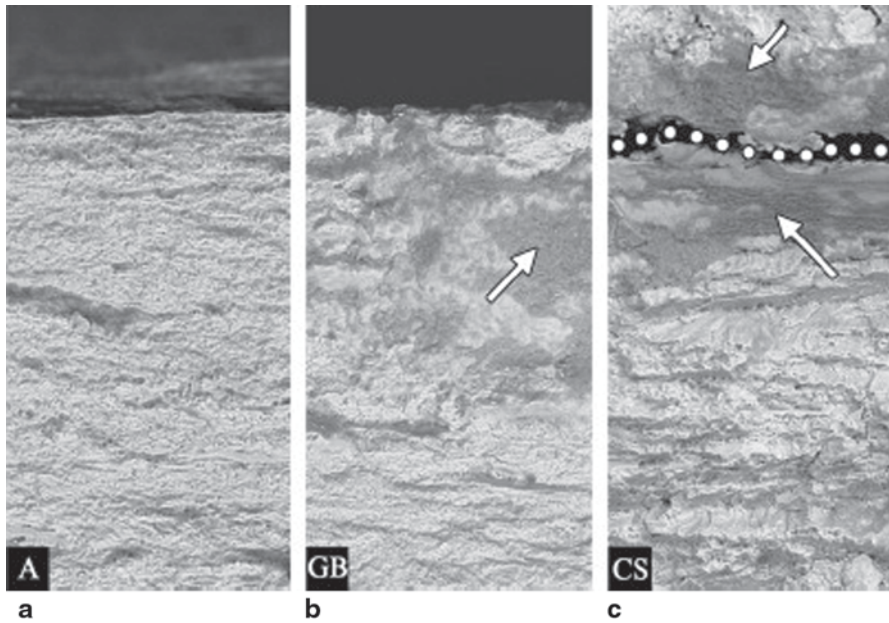
Fig. 5.21 Fatigue crack morphologies close to the substrate surfaces at approximately 3 mm from the sample edges for **a** as-received *(A),* **b** grit-blasted *(GB),* and **c** cold-sprayed *(CS)* samples. The fracture morphology of *GB* and *CS* substrates was obliterated by crushed abrasive particles near the substrate surface (contact wear-like, indicated by *arrows*). (Cizek et al. 2013)

is believed that the decrease in life may be due to a vertical cracking of the coatings followed by the crack transfer into the substrates and compensation of the residual peening stresses in the coatings by induction of tensile stresses in the substrates. Fractography analysis, as shown in Fig. 5.21, of the deposits enabled differentiating the areas of the fracture surfaces that underwent the cyclic opening/closing from the areas of the final rupture; the areas were characterized by signs of contact wear of the fracture surfaces, causing obliteration of the initial structure; due to the obliteration, the crack initiation sites and propagation directions could not be accurately identified in the coatings.

Price et al. (2006) studied the effect of cold spray deposition of titanium coating on Ti6Al4V on fatigue life of the coated samples. The fatigue lives of the as-received and GB materials, both before and after coating, were experimentally studied. A 15 % reduction in fatigue endurance was observed after application of the coating on the substrate; however, no significant reduction was observed on its application to the GB substrate. The compressive residual stresses reported through cold spray titanium coatings were too low to prevent fatigue crack formation and advancement. It should be considered that Price et al. (2006) have reported negligible compressive residual stresses on the deposited materials and the coated samples. The SEM observations also showed delamination in deposited material after fatigue test, which represented no or a little contribution of the deposited materials to the fatigue test.

On the other hand, Sansoucy et al. (2007), in particular, worked on bending fatigue and the bonding strength of the Al–Co–Ce coatings. The results show that Al–Co–Ce coatings improved the fatigue behavior of Al-2024-T3 specimens compared to uncoated specimens.

5.5 Concluding Remarks

The mechanism of formation of residual stress in a cold spray process was discussed. Methods for quantifying the magnitude of these stresses were reviewed, and experimental measurements for the case of aluminum and magnesium were presented. The theoretical foundation for modeling the impact of particles with substrate was studied in detail, and two approaches were laid out thoroughly. Finally, the benefit of residual stresses induced by cold spray coating on fatigue life enhancement of the substrate was explored.

Following general conclusions may be drawn from above presentation:

- Compressive residual stresses are formed because of an elastically bounded local plasticity induced by high-impact energy of coating particles with the substrate.
- Parameters such as impact velocity, particle size, material properties of particles and substrate, process temperature, standoff distance, initial as-received residual stresses, and particle shape are the controlling factors of the resulting residual stress due to impact.
- The magnitude of residual stress induced by cold spray depends heavily on the choice of the substrate and coating powder. While harder aluminum particle coating on aluminum substrate created a large residual stress leading to a significant fatigue life enhancement, the case of titanium showed the opposite.
- Coating temperature can result in an annealing process after the particle adhered to the surface and cooled down to normal temperature. This annealing process results in relaxation of residual stress. An after-simulation annealing correction calculation was proposed which showed better results when compared to measurement.

References

Abaqus 6.12–1. 2012. Analysis user's manual, simulia. http://asm.matweb.com/search/SpecificMaterial.asp?bassnum=MA7075T6. Accessed 1 June 2015.

ASM. 1989. *ASM Metal Handbooks*. Properties and Selection: Nonferrous Alloys and Special-Purpose Materials, vol. 2.

ASTM standard B593–96. 2009. Standard test method for bending fatigue testing for copper-alloy spring materials.

ASTM standard E739–10. 2010. Standard practice for statistical analysis of linear or linearized stress life (S–N) and strain life (e–N) fatigue data.

Albinmousa, J., H. Jahed, and S. Lambert. 2011. Cyclic axial and cyclic torsional behaviour of extruded AZ31B magnesium alloy. *International Journal of Fatigue* 33 (11): 1403–1416.

Allen, T. 2003. *Powder sampling and particle size determination*. 1st ed. Elsevier Science. ISBN: 044451564X.

Assadi, H., F. Gärtner, T. Stoltenhoff, and H. Kreye. 2003. Bonding mechanism in cold gas spraying. *Acta Materialia* 51 (15): 4379–4394.

Bagherifard, S., I. Fernàndez Parienete, R. Ghelichi, M. Guagliano, and S. Vezzù. 2010a. Effect of shot peening on residual stresses and surface work-hardening in cold sprayed coatings. *Key Engineering Materials* 417:397–400.

Bagherifard, S., R. Ghelichi, and M. Guagliano. 2010b. A numerical model of severe shot peening (SSP) to predict the generation of a nanostructured surface layer of material. *Surface and Coatings Technology* 204 (24): 4081–4090.

Benck, R. F. 1976. Quasi-static tensile stress strain curves–II, rolled homogeneous armor, DTIC Document.

Brar, N. S., V. S. Joshi, B. W. Harris, M. Elert, M. D. Furnish, W. W. Anderson, W. G. Proud, and W. T. Butler. 2009. *Constitutive model constants for Al7075-T651 and Al7075-T6*. Aip conference proceedings.

Cadney, S., M. Brochu, P. Richer, and B. Jodoin. 2008. Cold gas dynamic spraying as a method for freeforming and joining materials. *Surface and Coatings Technology* 202 (12): 2801–2806.

Champagne, V. K. 2007. *The cold spray materials deposition process: Fundamentals and applications*. 1st ed. Cambridge: Woodhead Publishing Limited. ISBN: 9781845691813.

Cizek, J., O. Kovarik, J. Siegl, K. A. Khor, and I. Dlouhy. 2013. Influence of plasma and cold spray deposited Ti Layers on high-cycle fatigue properties of Ti6Al4V substrates. *Surface and coatings technology* 217:23–33.

Dixon, W. J., and F. J. Massey. 1969. *Introduction to statistical analysis*. New York: McGraw-Hill.

Dykhuizen, R. C., and M. F. Smith. 1998. Gas dynamic principles of cold spray. *Journal of Thermal Spray Technology* 7 (2): 205–212.

Fine, M. E. 1964. *Introduction to phase transformations in condensed systems. Macmillan Materials Science Series*. New York: Macmillan Comp.

Ghelichi, R. 2012. Cold spray coating aimed nanocrystallization: Process characterization and fatigue strength assessment, PhD Thesis, Polytechnic University of Milan.

Ghelichi, R., S. Bagherifard, M. Guagliano, and M. Verani. 2011. Numerical simulation of cold spray coating. *Surface and Coatings Technology* 205 (23): 5294–5301.

Ghelichi, R., D. MacDonald, S. Bagherifard, H. Jahed, M. Guagliano, and B. Jodoin. 2012. Microstructure and fatigue behavior of cold spray coated Al5052. *Acta Materialia* 60 (19): 6555–6561.

Ghelichi, R., S. Bagherifard, D. Mac Donald, M. Brochu, H. Jahed, B. Jodoin, and M. Guagliano. 2014a. Fatigue strength of Al alloy cold sprayed with nanocrystalline powders. *International Journal of Fatigue* 65:51–57.

Ghelichi, R., S. Bagherifard, D. MacDonald, I. Fernandez-Pariente, B. Jodoin, and M. Guagliano. 2014b. Experimental and numerical study of residual stress evolution in cold spray coating. *Applied Surface Science* 288:26–33.

Greving, D. J., E. F. Rybicki, and J. R. Shadley. 1994. Through-thickness residual stress evaluations for several industrial thermal spray coatings using a modified layer-removal method. *Journal of thermal spray technology* 3 (4): 379–388.

Grujicic, M., C. Tong, W. S. DeRosset, and D. Helfritch. 2003. Flow analysis and nozzle-shape optimization for the cold-gas dynamic-spray process. *Proceedings of the Institution of Mechanical Engineers, Part B: Journal of Engineering Manufacture* 217 (11): 1603–1613.

Grujicic, M., C. L. Zhao, W. S. DeRosset, and D. Helfritch. 2004a. Adiabatic shear instability based mechanism for particles/substrate bonding in the cold-gas dynamic-spray process. *Materials & design* 25 (8): 681–688.

Grujicic, M., C. L. Zhao, C. Tong, W. S. DeRosset, and D. Helfritch. 2004b. Analysis of the impact velocity of powder particles in the cold-gas dynamic-spray process. *Materials Science and Engineering: A* 368 (1): 222–230.

Jeong, C. Y., and S. Ha. 2008. Fatigue properties of Al–Si casting alloy with cold sprayed Al/SiC coating. *International Journal of Cast Metals Research* 21 (1–4): 235–238.

Johnson, G. R., and W. H. Cook. 1983. *A constitutive model and data for metals subjected to large strains, high strain rates and high temperatures*. Proceedings of the 7th international symposium on ballistics.

Kalatehmollaei, E., H. Mahmoudi-Asl, and H. Jahed. 2014. An asymmetric elastic–plastic analysis of the load-controlled rotating bending test and its application in the fatigue life estimation of wrought magnesium AZ31B. *International Journal of Fatigue* 64:33–41.

Kovářík, O., J. Siegl, and Z. Procházka. 2008. Fatigue behavior of bodies with thermally sprayed metallic and ceramic deposits. *Journal of thermal spray technology* 17 (4): 525–532.

Kumar, S., G. Bae, K. Kang, S. Yoon, and C. Lee. 2009. Effect of powder state on the deposition behaviour and coating development in kinetic spray process. *Journal of Physics D: Applied Physics* 42 (7): 075305.

Lemaitre, J., and J.-L. Chaboche. 1990. *Mechanics of solid materials*. New York: Cambridge University Press.

Li, C.-J., W.-Y. Li, and H. Liao. 2006. Examination of the critical velocity for deposition of particles in cold spraying. *Journal of Thermal Spray Technology* 15 (2): 212–222.

LS-DYNA3D. 1999. User's manual. Ver. 950. Livermore software technology corporation, Livermore, California.

Los Alamos. 1969. "Selected Hugoniots", Group GMX-6, Los Alamos Scientific Lab., LA-4167–MS.

Luzin, V., K. Spencer, and M. X. Zhang. 2011. Residual stress and thermo-mechanical properties of cold spray metal coatings. *Acta Materialia* 59 (3): 1259–1270.

Maev, R. G., and V. Leshchinsky. 2008. *Introduction to low pressure gas dynamic spray: Physics & technology*. Wiley-VCH Verlag GmbH.

Mahmoudi, H. 2012. MSc. thesis. Mechanical and Mechatronics Engineering Department, University of Waterloo.

Mahmoudi, H., H. Jahed, and J. Villafuerte. 2012. The effect of cold spray coating on fatigue life of AZ31B. 9th International conference on magnesium alloys and their applications, Vancouver, BC.

McCune, R. C., W. T. Donlon, O. O. Popoola, and E. L. Cartwright. 2000. Characterization of copper layers produced by cold gas-dynamic spraying. *Journal of Thermal Spray Technology* 9 (1): 73–82.

Moridi, A., S. M. Hassani-Gangaraj, M. Guagliano, and S. Vezzu. 2014. Effect of cold spray deposition of similar material on fatigue behavior of Al 6082 alloy. *Fracture and Fatigue* 7:51–57 (Springer).

Najafi, A., and M. Rais-Rohani. 2011. Mechanics of axial plastic collapse in multi-cell, multi-corner crush tubes. *Thin-Walled Structures* 49 (1): 1–12.

Papyrin, A., V. Kosarev, K. V. Klinkov, A. Alkhimov, and V. M. Fomin. 2006. *Cold spray technology*. (A. Papyrin. ed.). Elsever.

Pierazzo, E., N. Artemieva, E. Asphaug, E. C. Baldwin, J. Cazamias, R. Coker, G. S. Collins, D. A. Crawford, T. Davison, D. Elbeshausen, K. A. Holsapple, K. R. Housen, D. G. Korycansky, and K. WÜNnemann. 2008. Validation of numerical codes for impact and explosion cratering: Impacts on strengthless and metal targets. *Meteoritics & Planetary Science* 43 (12): 1917–1938.

Price, T. S., P. H. Shipway, and D. G. McCartney. 2006. Effect of cold spray deposition of a titanium coating on fatigue behavior of a titanium alloy. *Journal of Thermal Spray Technology* 15 (4): 507–512.

Ramakrishnan, K. N. 2000. Modified Rosin Rammler equation for describing particle size distribution of milled powders. *Journal of Materials Science Letters* 19 (21): 1903–1906.

Robert, C. 1984. *CRC handbook of chemistry and physics*. Boca Raton: CRC Press.

RosIn, P. 1933. The laws governing the fineness of powdered coal. *Journal of the Institute of Fuel* 7:29–36.

Rybicki, E. F., J. R. Shadley, Y. Xiong, and D. J. Greving. 1995. A cantilever beam method for evaluating Young's modulus and Poisson's ratio of thermal spray coatings. *Journal of Thermal Spray Technology* 4 (4): 377–383.

Sansoucy, E., G. E. Kim, A. L. Moran, and B. Jodoin. 2007. Mechanical characteristics of Al-Co-Ce coatings produced by the cold spray process. *Journal of Thermal Spray Technology* 16 (5–6): 651–660.

Shayegan, G., H. Mahmoudi, R. Ghelichi, J. Villafuerte, J. Wang, M. Guagliano, and H. Jahed. 2014. Residual stress induced by cold spray coating of magnesium AZ31B extrusion. *Materials & Design* 60:72–84.

Spencer, K., V. Luzin, N. Matthews, and M. X. Zhang. 2012. Residual stresses in cold spray Al coatings: The effect of alloying and of process parameters. *Surface and Coatings Technology* 206 (19–20): 4249–4255.

Totten, G. E. 2002. *Handbook of residual stress and deformation of steel*. Ohio: ASM International, Materials Park.

Tsui, Y. C., and T. W. Clyne. 1997. An analytical model for predicting residual stresses in progressively deposited coatings part 1: Planar geometry. *Thin Solid Films* 306 (1): 23–33.

Weast R. C., and D. R. Lide. 1984. *CRC handbook of chemistry and physics. University of Rhode Island. Coastal Resources Center*. Cleveland: CRC Press.